Supporting Information for

Dendritic, Transferable, Strictly Monolayer MoS_2 Flakes Synthesized on $SrTiO_3$ Single Crystals for Efficient Electrocatalytic Applications

Yu Zhang,[†,‡] Qingqing Ji,[‡] Gao-Feng Han,[ξ] Jing Ju,[δ] Jianping Shi,[†,‡] Donglin Ma,[‡] Jingyu Sun,[‡] Yanshuo Zhang,[†,‡] Minjie Li,[‡] Xing-You Lang,[ξ] Yanfeng Zhang,[†,‡*] Zhongfan Liu[‡]

[†] Department of Materials Science and Engineering, College of Engineering, Peking University, Beijing 100871, People's Republic of China

[‡] Center for Nanochemistry (CNC), Beijing National Laboratory for Molecular Sciences, College of Chemistry and Molecular Engineering, Peking University, Beijing 100871, People's Republic of China

[ξ] Key Laboratory of Automobile Materials (Jilin University), Ministry of Education, and School of Materials Science and Engineering, Jilin University, Changchun 130022, People's Republic of China

[δ] State Key Laboratory of Rare Earth Materials Chemistry and Applications, College of Chemistry and Molecular Engineering, Peking University, Beijing 100871, People's Republic of China

[*] Address correspondence to: yanfengzhang@pku.edu.cn

1. **Experiment setup of MoS_2 growth by LPCVD system.**

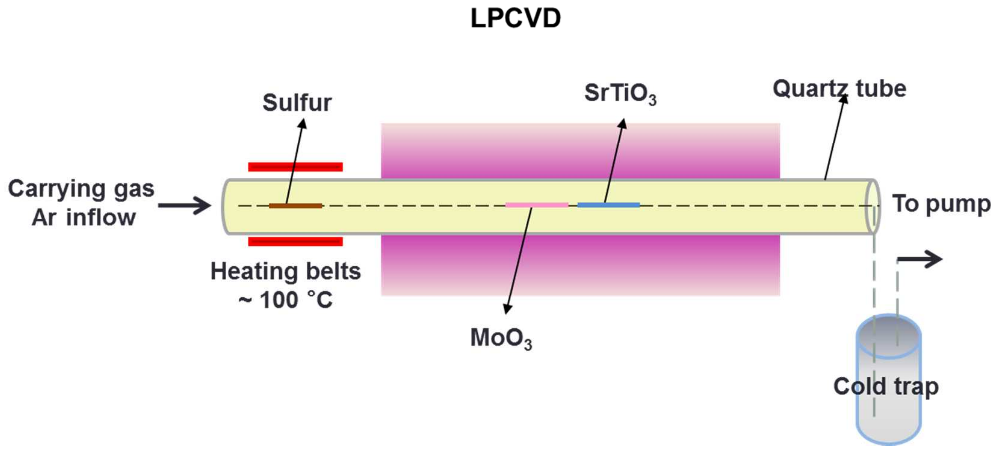

Figure S1 Schematic view of the utilized LPCVD system and the experimental setup for MoS_2 growth on STO(100) and STO(111) substrates.

In the LPCVD growth process, sulfur powder was mildly sublimated at ~100 °C and carried by Ar (50 sccm) gas flow, keeping the subsequent growth zone in a sulfur-rich atmosphere. The MoO_3 powder and STO substrates were heated to ~530 °C, ~880 °C, respectively. The tube furnace was pumped down to ~30 Pa to realize a LPCVD condition.

2. SEM images of LPCVD synthesized MoS_2 flakes on STO (100).

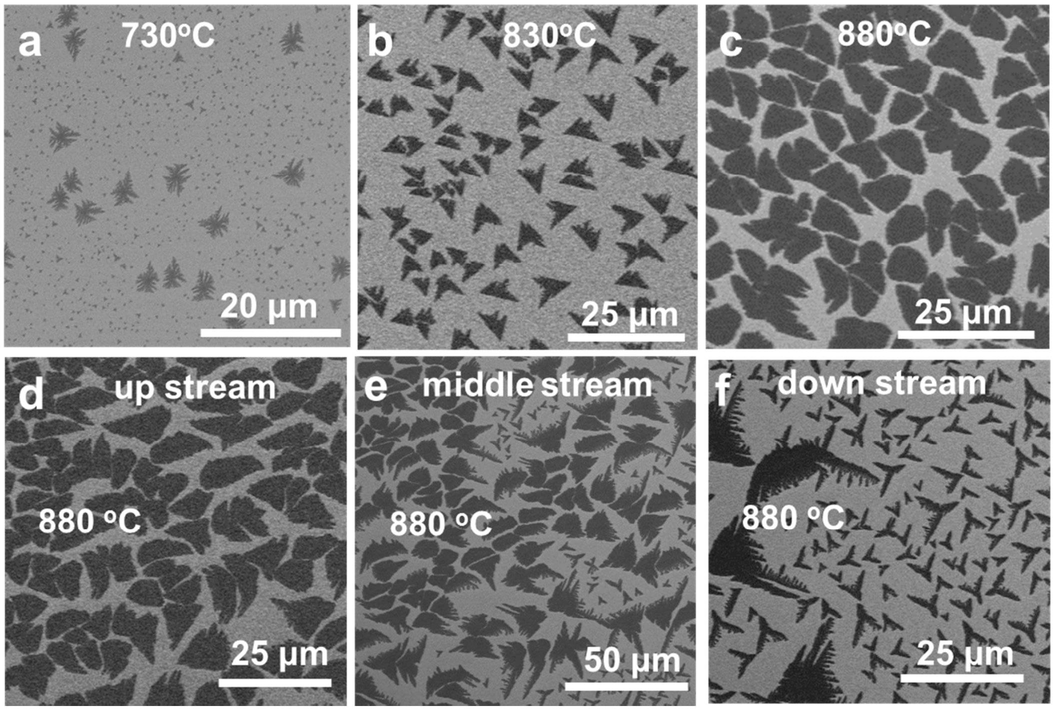

Figure S2 Large scale SEM morphologies of LPCVD synthesized MoS_2 on STO (100). (a-c) SEM images of different shapes of MoS_2 flakes synthesized at various growth temperature of 730°C, 830°C and 880°C, respectively. (d-f) SEM morphologies of three MoS_2 samples with various coverage and distinct flake shape, synthesized under the same growth procedure (growth temperature 880°C) but with increased source-substrate distances (D_{ss}) of 10.0 cm, 10.5cm and 11.0 cm, respectively.

Based on the above results, it can be inferred that, the growth temperature and the source-substrate distances (D_{ss}) are significant parameters for modulating the morphology of MoS_2. A high growth temperature usually results in compact MoS_2 flakes possessing rather sharp edges, as well as increased domain size. Moreover, a relative large precursor-substrate distance usually corresponds to rather small flake sizes and fractal flakes.

3. **Crystal structures of two kind crystal faces of STO and the SEM images of synthesized MoS_2 on STO(111).**

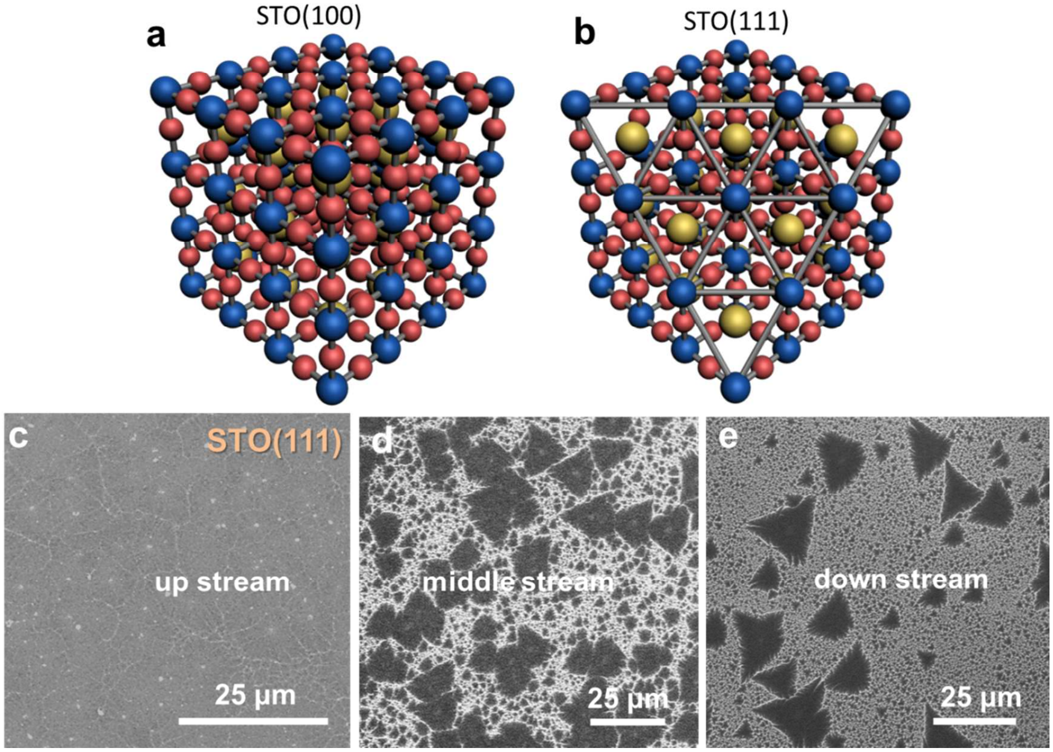

Figure S3 LPCVD synthesis of MoS_2 on STO (111). (a-b) Crystal structures of STO (100) and STO (111), respectively. (c-e) Large scale SEM morphologies of MoS_2 samples synthesized on STO (111) under the same growth procedure (growth temperature 880°C) but with different source-substrate distances (D_{ss}) of 10.0 cm, 10.5 cm and 11.0 cm, respectively, with the formation of nearly monolayer film (c) and submonolayer flakes (d,e).

It is also find that, MoS_2 flakes can be synthesized on the single crystal substrate of STO (111). And the MoS_2 flakes on STO (111) usually show more regular shapes than the growth on STO(100), as evidenced by the SEM images shown in Fig. S3d, e.

4. **SEM morphologies of MoS_2 directly grown on STO and sapphire under the same growth batch.**

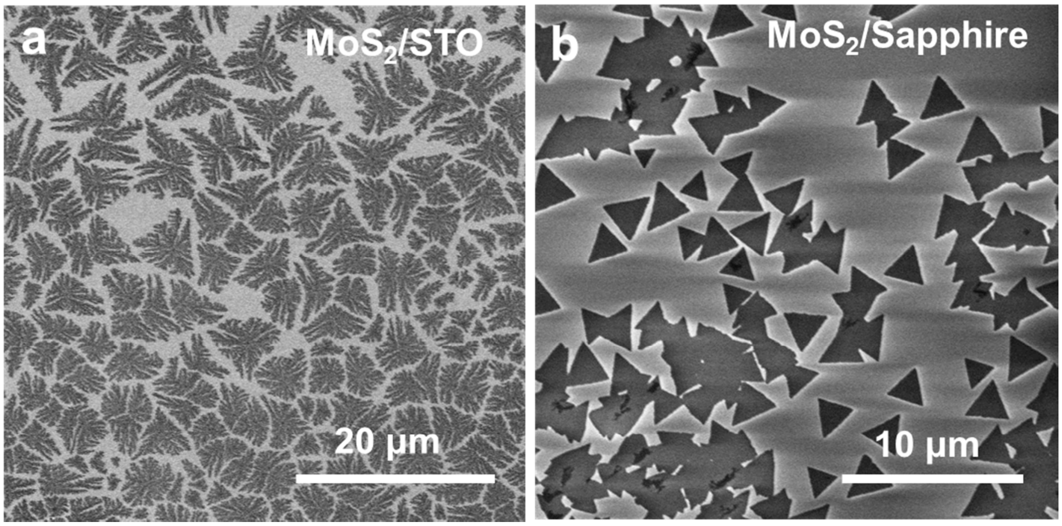

Figure S4 SEM morphologies of MoS_2 directly grown on STO and sapphire under the same growth batch. (a, b) MoS_2 on STO and on sapphire, respectively. The growth temperature of the synthesized samples was set at ~880°C, and the precursor substrate distance (D_{ss}) was also set at a reasonable value.

Comparative SEM results indicate that, the generally synthesized MoS_2 on STO (at a medium growth temperature) has a special fractal morphology, which is considered to be mediated by a relative strong interface interaction between MoS_2 and STO, with regard to the system of MoS_2 on sapphire.

5. AFM results of as-grown dendritic MoS_2 flakes.

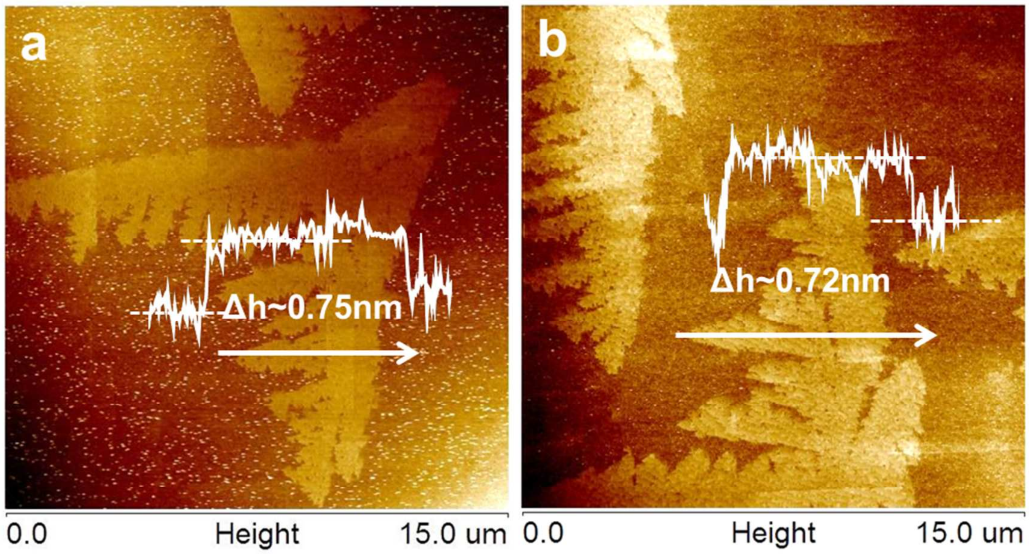

Figure S5 AFM images and corresponding height profiles along the white arrows of dendritic MoS_2 flakes in both (a) and (b)..

It is shown that, AFM results exhibit the morphologies of dendritic MoS_2 flakes, mmeanwhile the height profiles manifest their monolayer feature.

6. **Raman and PL measurments of bare STO substrates.**

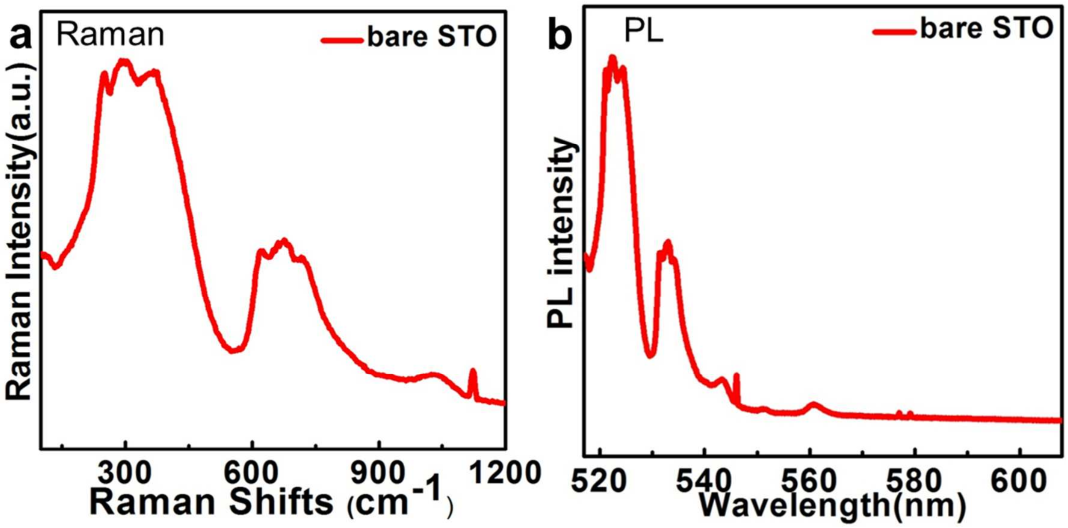

Figure S6 Raman (a) and PL (b) spectra of the bare STO substrate.

It is found that, from 300 cm^{-1} to 750 cm^{-1} (from 500 nm to 550 nm), the characteristic peaks of the bare STO substrate is very strong, and the Raman peaks of MoS_2 cannot be identified.

7. SEM morphlogies of transferred MoS_2 flakes with dendritic edges onto SiO_2/Si .

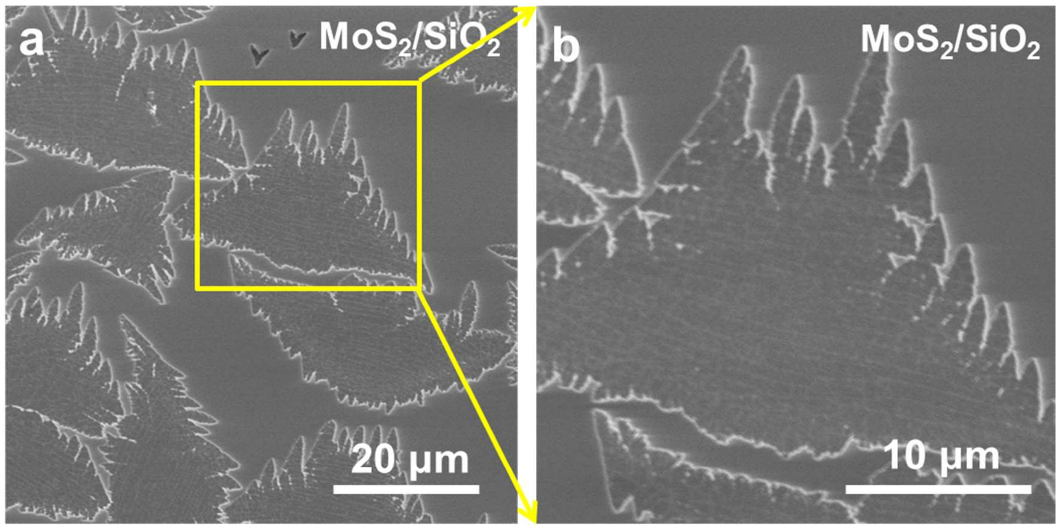

Figure S7 SEM images of MoS_2 flakes after transference onto SiO_2/Si showing the maintenance of the dendritic edges of the flakes. (a) Large scale SEM image of transferred MoS_2 on SiO_2/Si. (b) Zoom in of the yellow square region in (a).

The SEM images show that, the MoS_2 flakes can keep their original shapes even after the transfer process. Another interesting thing is that inside the flake, some white line shaped contrasts can be noticed and regarded as MoS_2 wrinkles, probably arising from the duplication of the steps of the STO substrate. This fact provides side evidence of the perfect transfer process, considering that the transferred MoS_2 flakes showing almost no broken, bending or folding.

8. SEM images of nearly complete monolayer MoS_2 transferred onto SiO_2/Si.

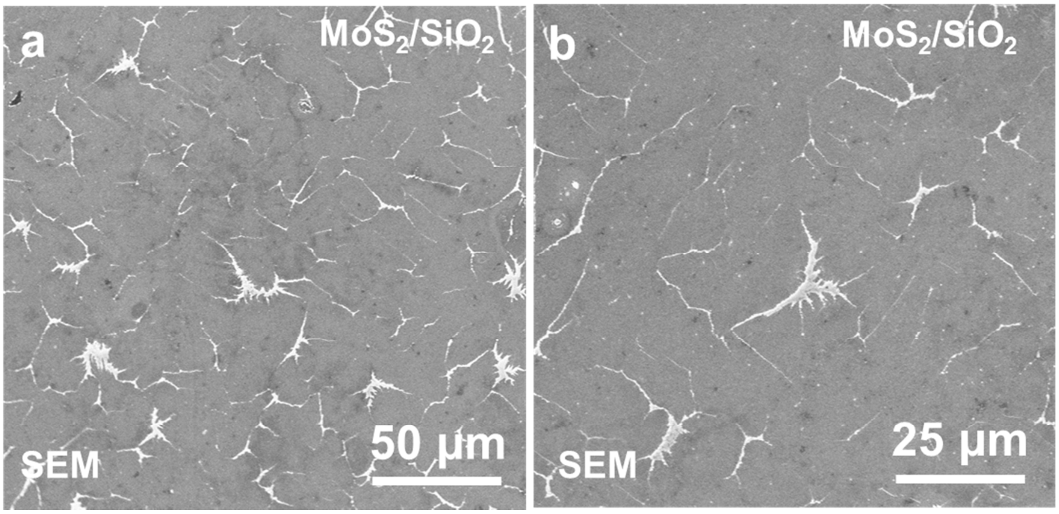

Figure S8 SEM images of nearly complete monolayer MoS_2 after transference onto SiO_2/Si in both (a) and (b).

The SEM results of transferred MoS_2 reveal that the complete monolayer MoS_2 on STO can be transferred intact onto SiO_2/Si.

9. Optical photographs of monolayer MoS_2 transferred on quartz.

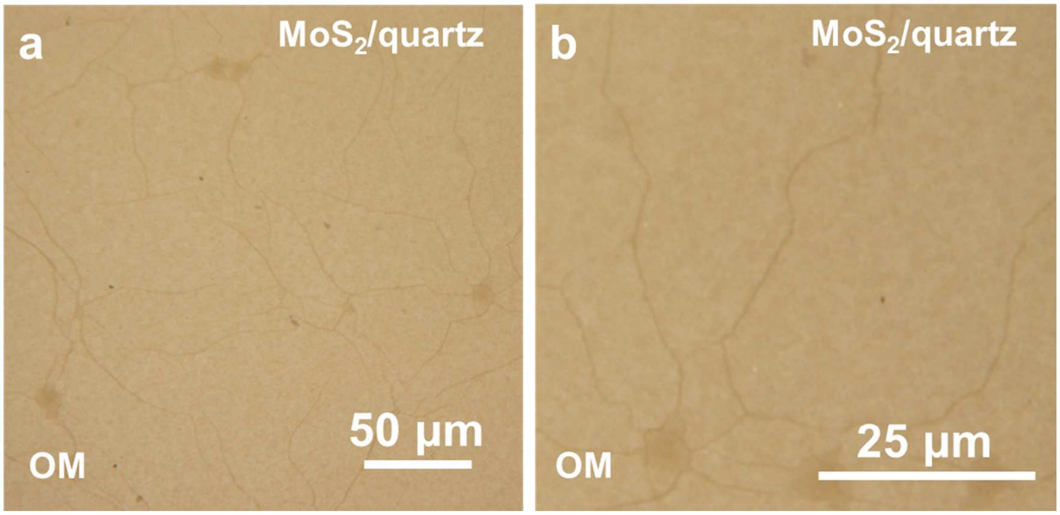

Figure S9 Optical photographs of monolayer MoS_2 transferred on quartz. (a,b) Optical photographs of different scales MoS_2 on quartz.

The OM results of transferred MoS_2 indicate that, the MoS_2 on STO can be transferred intact onto quartz.

10. High-resolution transmission electron microscopy (HRTEM) characterization of monolayer MoS_2 flakes.

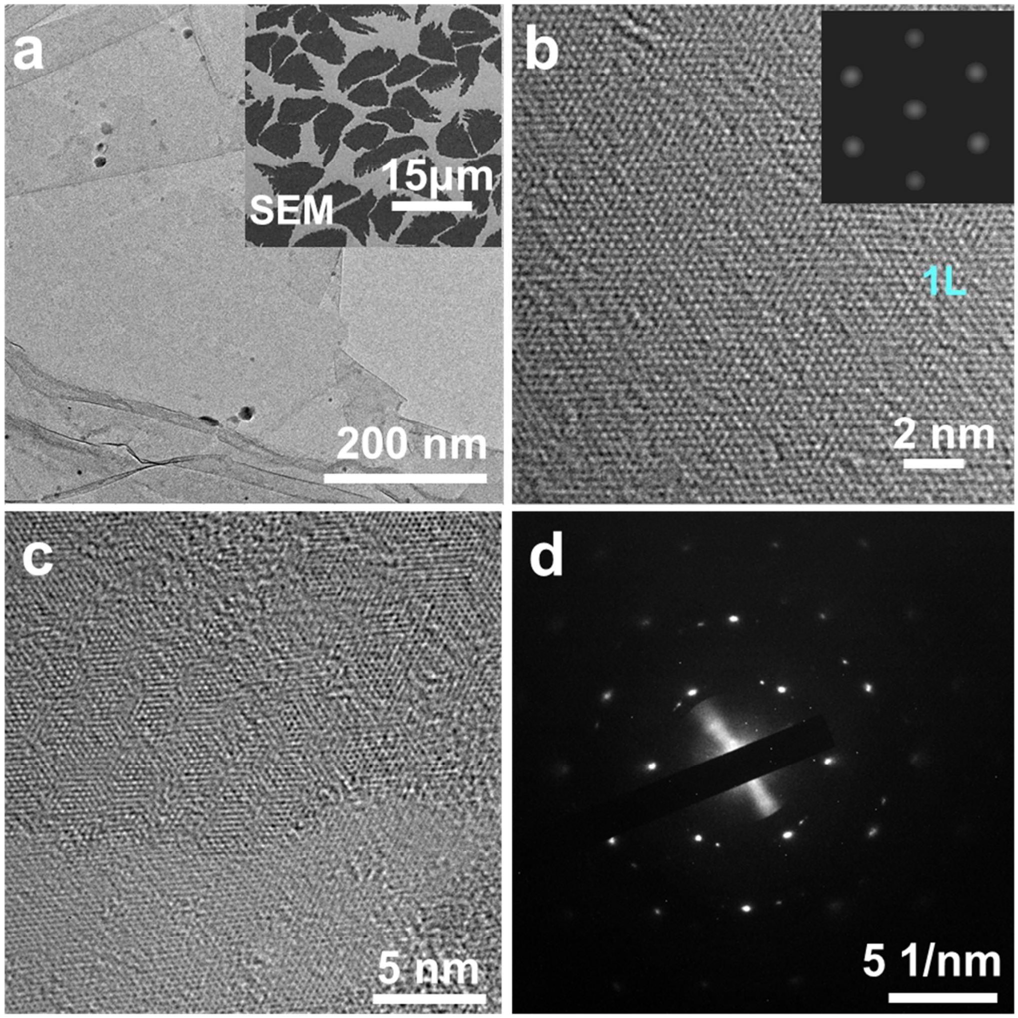

Figure S10 High-resolution transmission electron microscopy (HRTEM) characterization of monolayer MoS_2 flakes. (a) Folded edge of the monolayer MoS_2 with the SEM image of the sample as an inset。(b) HRTEM image and its FFT of monolayer MoS_2. (c) HRTEM images of an area consisting of monolayer (lower part) and stacked bilayer (upper part) MoS_2. (d) Corresponding SAED pattern of (c) showing two sets of diffraction spots.

The HRTEM results demonstrate the monolayer thickness and high crystal quality of the synthesized MoS_2 on STO.

11. Nyquist plots of the three MoS_2 samples for the HER measurements.

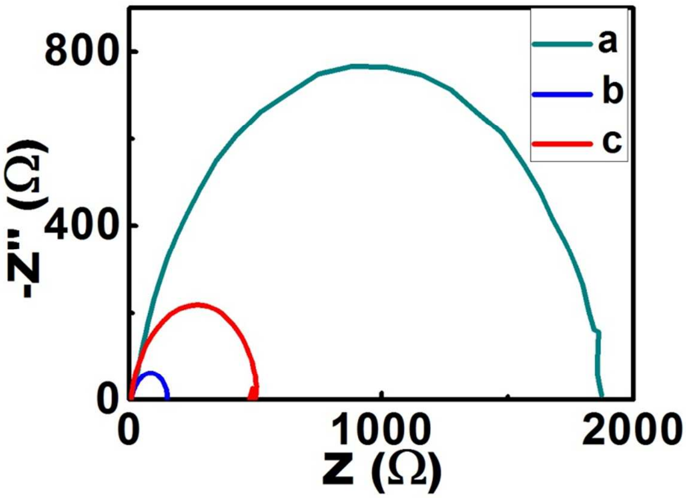

Figure S11 Nyquist plots of the three MoS_2 samples for the HER measurements.

The Nyquist plots show the charge-transfer resistance (R_{CT}) of the three samples are 150 Ω, 400 Ω and 1750 Ω, respectively.